Electrical Soliton Oscillator

David S. Ricketts, *Student Member, IEEE*, Xiaofeng Li, *Student Member, IEEE*, and Donhee Ham, *Member, IEEE*

***Abstract*—This paper introduces the first robust self-sustained electrical soliton oscillator. It self-starts by amplifying background noise to produce a stable train of periodic electrical soliton pulses. The oscillator is made possible by coupling a nonlinear transmission line with a unique amplifier that tames the instability-prone soliton dynamics. Two experimental prototypes, built at the discrete level, fully demonstrate the detailed operation of the circuit. The soliton oscillator is an electrical analog of optical soliton mode-locked systems.**

***Index Terms*—Electrical solitons, mode-locking, nonlinear transmission lines (NLTLs), oscillators, pulse generation, soliton mode locking, soliton oscillators, solitons.**

I. Introduction

SOLITONS ARE a special class of pulse-shaped waves that propagate without changing their shape in nonlinear dispersive media [1]–[5]. A balancing mechanism between nonlinearity and dispersion is responsible for the soliton phenomena.

Nature offers a variety of soliton examples. The first-reported soliton was a mono-pulse water wave in a narrow canal where the shallow water possessed both nonlinearity and dispersion [5], [6]. A mechanical spring-mass lattice can also act as a nonlinear dispersive medium, propagating solitons in the form of lattice waves [7], [8]. The optical fiber is yet another example of a nonlinear dispersive medium where optical solitons are observed [9].

In electronics, the nonlinear transmission line (NLTL) serves as a nonlinear dispersive medium that propagates voltage solitons [10], [11]. These electrical solitons on the NLTL have been actively investigated over the last 40 years, particularly in the microwave domain, for the generation of sharp pulse [11], [17] and their application to microwave sampling [11], [18]–[20]. In these past studies, the NLTL has been predominantly used as a *two*-port system where a high-frequency input is required to generate a sharp soliton output through a transient process.

One meaningful extension of the past two-port NLTL works would be to construct a *one*-port self-sustained electrical soliton oscillator by properly combining the NLTL with an amplifier (positive active feedback). Such an oscillator would self-start by growing from ambient noise to produce a train of periodic electrical soliton pulses in steady state and, hence, would make a self-contained soliton generator that does not require an external high-frequency input. While such a circuit may offer a new direction in the field of electrical pulse generation, there has not been a *robust* electrical soliton oscillator reported to date, to the best of our knowledge. While Ballantyne *et al.* indeed demonstrated an NLTL-based soliton oscillator [21]–[23], its oscillations were not always reproducible, lacking robustness and controllability. The difficulty in constructing the one-port soliton oscillator arises because the NLTL's instability-prone soliton dynamics do not easily lend themselves to standard amplification techniques.

In this paper, we introduce the first robust electrical soliton oscillator. This circuit is made possible by combining the NLTL with a unique amplifier. This amplifier "tames" the instability-prone NLTL dynamics by utilizing an adaptive bias control in conjunction with its nonlinear transfer characteristic. The essential operating properties of our amplifier are remarkably similar to an amplifier developed by Cutler for an electrical linear-pulse (*nonsoliton*) oscillator using a *linear* transmission line [24]. Due to the nonlinearity in the NLTL, however, the signal dynamics and stability/design issues of our soliton oscillator are fundamentally different from those of Cutler's linear-pulse oscillator.

In [25], we have recently reported the preliminary results from a megahertz prototype of our soliton oscillator. The paper presented here is a complete account of the novel soliton oscillator concept with new, extensive experimental verification of its governing principles and detailed operation using the prototype of [25]. In addition, a new microwave prototype is demonstrated to illustrate the generality of the soliton oscillator concept and feasibility of higher frequency designs. We start by briefly reviewing the NLTL and its soliton dynamics in Section II as the background. Section III discusses a feasible soliton oscillator topology and its instability mechanisms. In Section IV, we describe the operating principles of our NLTL-based soliton oscillator that circumvents the instability issues, while the experimental demonstration is presented in Sections V and VI. Section VII juxtaposes our soliton oscillator with Cutler's linear-pulse oscillator to elucidate their fundamental differences.

II. NLTL and Electrical Solitons

Here, we briefly review the NLTL and soliton propagation on the NLTL to provide the necessary background.

As illustrated in Fig. 1(a), an NLTL can be constructed from a linear transmission line by periodically loading it with varactors, such as reverse-biased pn junction diodes or MOS capacitors [11]. Varactors are nonlinear capacitors whose capacitance changes with the applied voltage. An NLTL can be alternatively obtained by replacing linear capacitors of an artificial *LC* transmission line with varactors as shown in Fig. 1(b).

The NLTL is a nonlinear dispersive system. The nonlinearity originates from the varactors. The dispersion arises from the

Manuscript received May 31, 2005; revised August 6, 2005. This work was supported in part by IBM under a Faculty Partnership Award, by the National Science Foundation under ITR Grant NSF-ECS-0313143, by the National Science Foundation Nanoscale and Engineering Center, and by the Center for Nanoscale Structures.

The authors are with the Division of Engineering and Applied Sciences, Harvard University, Cambridge, MA 02138 USA (e-mail: donhee@deas.harvard.edu).

Digital Object Identifier 10.1109/TMTT.2005.861652

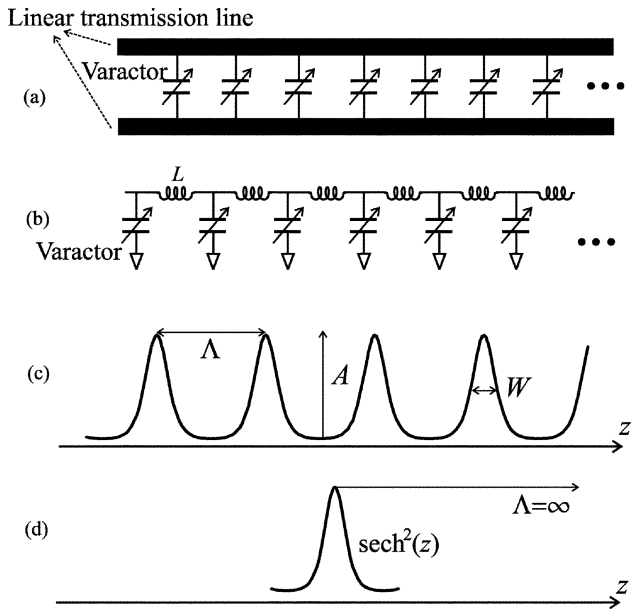

Fig. 1. (a) NLTL consisting of a linear transmission line and varactors. (b) Artificial NLTL. (c) General soliton wave formed on an infinitely long NLTL, which is a soliton pulse train, also known as a cnoidal wave. (d) The mono-pulse case.

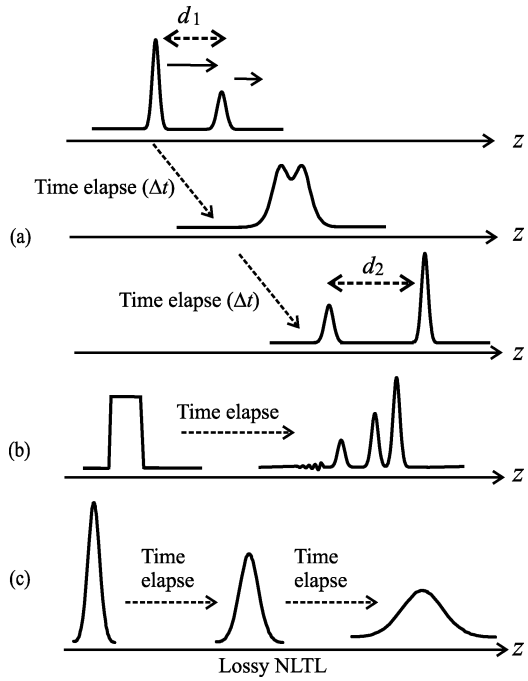

Fig. 2. (a) Hypothetical depiction of amplitude-dependent soliton speeds and nonlinear soliton collision on an NLTL. $d_1 \neq d_2$. (b) Simulated breakup of a square pulse into multiple solitons on the NLTL. (c) Hypothetical illustration of a damping soliton on a lossy NLTL.

structural periodicity. If the nonlinearity balances out the dispersion in the NLTL, a special type of pulse-shaped voltage wave can propagate down the line, while maintaining its shape. This is an electrical soliton [10], [11]. Fig. 1(c) shows a general soliton wave formed on an infinitely long NLTL, which is a train of periodic solitons. This waveform is also known as a *cnoidal wave* [3]–[5]. There are an infinite number of possible cnoidal waves that can form on the NLTL by varying the amplitude A, pulse spacing Λ, and the pulsewidth W. Initial and/or boundary conditions will determine the specific cnoidal waves that can propagate on the line. Fig. 1(d) shows the special mono-pulse case.

In addition to maintaining their shape, solitons on the NLTL possess other important properties [3]–[5]. To begin with, a taller soliton travels faster than a shorter one on the NLTL. Due to this amplitude-dependent speed, as shown in Fig. 2(a), a taller soliton originally placed behind a shorter one catches up with the shorter one and moves ahead of it after a collision. Another important set of properties is observed in this collision process. *During* the collision [middle of Fig. 2(a)], the two solitons do not linearly superpose (nonlinear collision), and as a result experience a significant amount of amplitude modulation. *After* the collision [bottom of Fig. 2(a)], the two solitons return to their original shapes, however, they have acquired a permanent time (phase) shift due to the nonlinear collision shown by the difference in d_1 and d_2 in Fig. 2(a) (with no time shift, d_1 and d_2 would be equal, since the time elapse before and after the collision is the same). These soliton properties, i.e., amplitude-dependent speed, amplitude modulation during the nonlinear collision, and phase modulation after the nonlinear collision, make the NLTL dynamics instability-prone, creating an adverse design environment for the soliton oscillator, as we will detail later.

Nonsoliton waves can also travel on the NLTL as well, but only by changing their shape into a soliton(s) in the course of propagation. A pulse close to the soliton shape will be sharpened into a single soliton while shedding extra energy in the form of a dispersive tail (ringings). A pulse that is significantly different from the soliton shape will break up into multiple solitons of different amplitudes and a dispersive tail. Once a soliton or solitons are formed, they propagate without further sharpening or breakup. Fig. 2(b) illustrates a simulated example in which a square pulse input on the NLTL breaks up into multiple soliton pulses. This soliton-forming transient behavior has been positively exploited for sharp soliton pulse generation in the two-port NLTL scheme [11]. In the one-port NLTL oscillator design, the transient behavior can be detrimental (see Section III-B) or beneficial (see Section V-E).

Thus far, we have ignored the loss inherent in any practical NLTL. Therefore, a note should be made about lossy NLTLs and their dynamics. When a nonsoliton waveform travels down a lossy NLTL, it will be shaped into a single or multiple solitons through the sharpening and/or breakup processes, just like in the lossless case (while losing some energy in the process). Once the solitons are formed, they do not undergo any further sharpening or breakup, but do continue to lose energy in the course of propagation, decreasing in amplitude and speed while increasing in width, as shown in Fig. 2(c), which is a key signature of a damping soliton [26]. Although solitons change their shape on the lossy NLTL due to damping, they remain solitons, exhibiting the key properties such as amplitude-dependant speed, nonlinear collision and its aftereffects. It should be also mentioned that the distinctive dynamics between the soliton's damping and the nonsoliton's breakup/sharpening process provide an important criterion to determine when a soliton has actually formed on the lossy NLTL.

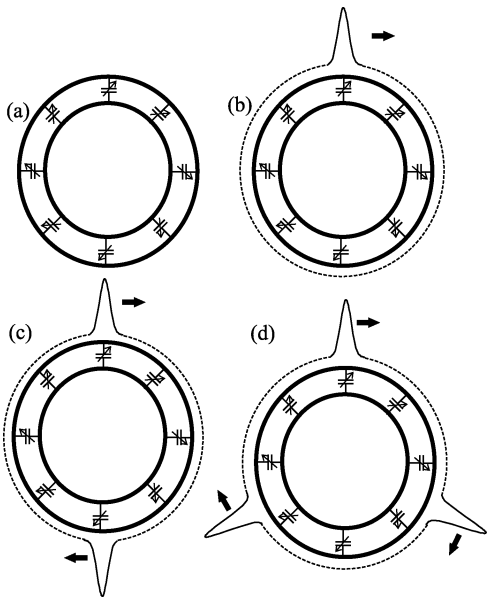

Fig. 3. (a) Ring NLTL. (b) Mode 1 ($l = \Lambda$). (c) Mode 2 ($l = 2\Lambda$). (d) Mode 3 ($l = 3\Lambda$).

III. NLTL Soliton Oscillator—Basic Topology and Instability Mechanisms

In this section, we present the basic structure of our NLTL soliton oscillator and identify its oscillation instability mechanisms. This section serves as a primer for Section IV, where we describe our working soliton oscillator that overcomes the instability issues.

A. Basic Topology

Let us first consider a closed-loop (ring) NLTL shown in Fig. 3(a). If only unidirectional propagation is allowed, then the possible soliton propagation modes (cnoidal wave modes) on the ring are the ones that satisfy the periodic boundary condition $l = n\Lambda$, $n = 1, 2, 3, \ldots$ [27], where l and Λ are the circumference of the ring and the spacing between neighboring solitons, respectively [for Λ, refer to Fig. 1(c)]. The first three soliton propagation modes formed on the ring are shown in Fig. 3(b)–(d).

Our starting idea to construct an electrical soliton oscillator is to break the ring NLTL and insert a noninverting amplifier, as shown in Fig. 4. The purpose of the amplifier is to enable initial startup from noise and to compensate for system loss in the steady state (as is commonly done in sinusoidal oscillators, e.g., [28] and [29]). The ultimate goal is for the circuit of Fig. 4 to self-generate and self-sustain one of the soliton propagation modes (Fig. 3) of the ring NLTL. The termination in Fig. 4 is needed to absorb energy: in the soliton oscillator, it is not energy but rather a voltage signal that circulates around the loop. The termination of the NLTL is not trivial since its characteristic impedance varies with signal voltage. A resistor with a value that is the average of the characteristic impedance seen by a desired signal is used in our approach. Resulting reflections from the imperfect termination will be treated as perturbations in this paper.

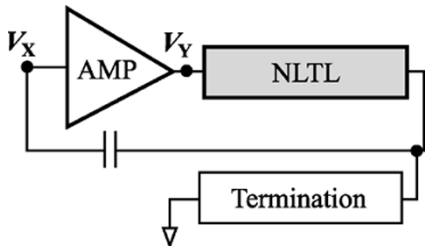

Fig. 4. Basic soliton oscillator topology.

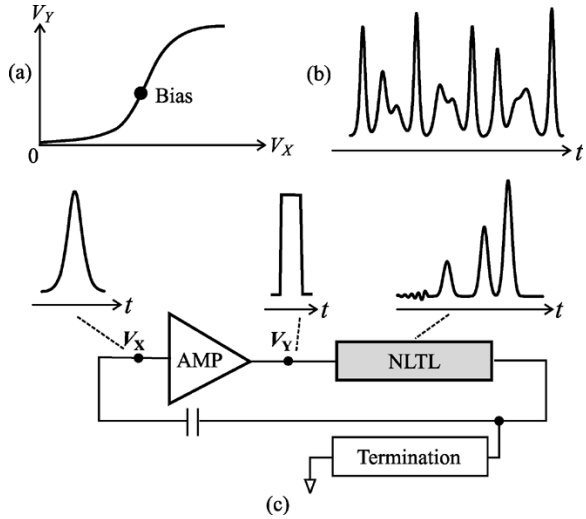

Fig. 5. (a) Transfer function of a voltage-limiting amplifier. (b) Simulated unstable oscillation of Fig. 4 with the voltage-limiting amplifier. (c) Impact of signal clipping or distortion.

As will be seen shortly, the proposed topology will indeed lead to an oscillation. However, the oscillation stability depends strongly on the amplifier characteristics. For the oscillator to generate a stable soliton pulse train, it is essential for the amplifier to "tame" the complex soliton dynamics of the NLTL, which, unfortunately, is not the case for standard amplification techniques.

B. Instability Mechanisms

In this section, we examine the dynamics of the circuit in Fig. 4 with two commonly used amplifiers. This will lead us to identify the instability mechanisms associated with the oscillator, which will be key to constructing our soliton oscillator discussed in Section IV.

Case I—Voltage-Limiting Amplifier: Let us first consider the case where a standard voltage-limiting noninverting amplifier is used in the circuit of Fig. 4. The transfer function of this amplifier is shown in Fig. 5(a). The amplifier is biased at a fixed operating point. Simulations show that the circuit of Fig. 4 indeed self-starts into oscillation, but the oscillation is unstable with significant amplitude and pulse repetition variations, often tending toward what appears to be a chaotic state, as shown in Fig. 5(b).

This oscillation instability arises from the signal clipping in the amplifier in connection with the unique NLTL properties. To see this, let us assume that a soliton pulse appears at the input of the amplifier at a certain time [V_X on the left-hand side of

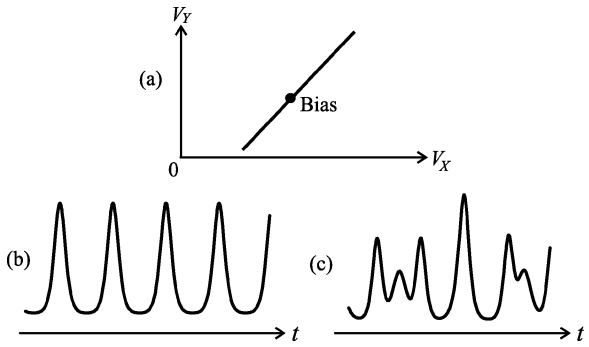

Fig. 6. (a) Linear amplifier transfer function. (b) Soliton oscillation of Fig. 4 with the linear amplifier [21]–[23]. (c) Depiction of other possible output waveforms [21]–[23].

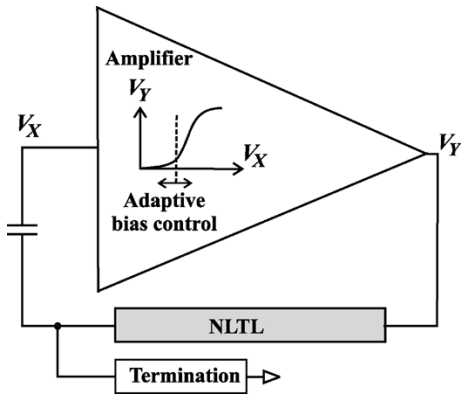

Fig. 7. Our soliton oscillator with the unique amplifier that performs the adaptive bias control.

Fig. 5(c)]. This soliton pulse, after passing through the amplifier, will turn into a square pulse due to the clipping of the amplifier [V_Y in Fig. 5(c)]. As explained in Section II, this square pulse will break up into several solitons with different amplitudes while propagating down the NLTL [see the rightmost waveform in Fig. 5(c)]. The multiple soliton pulses will travel at different speeds due to their amplitude-dependant speed, eventually appearing again at the input of the amplifier. This process repeats itself, creating many soliton pulses with various amplitudes in the loop. These soliton pulses propagate at different speeds and continually collide with one another. As discussed in Section II, these soliton collisions lead to phase/amplitude modulations making the oscillation unstable

Case II—Linear Amplifier: The discussion above shows that signal distortion has a negative impact on the oscillation stability, suggesting that one might be able to attain a stable soliton oscillation if signal distortion is mitigated. Ballantyne *et al.* [21]–[23] implemented such a system by using a linear amplifier whose transfer function is shown in Fig. 6(a). By using the linear amplifier and adding additional frequency-dependent loss to the NLTL, he could produce a periodic soliton pulse train as illustrated in Fig. 6(b). In the same system, however, other oscillations uncontrollably appeared with slight changes in gain, termination, or with external perturbations, indicating a lack of robustness. These waveforms sometimes contained multiple solitons with varying amplitudes/spacings and pulses continuously moved relative to one another and collided (see Fig. 6(c) for a depiction). While Ballantyne's system is invaluable for providing an opportunity to examine soliton dynamics, it is not able to reproduce a stable soliton pulse train, which is the goal of this study.

Identification of Three Instability Mechanisms: Ballantyne's work suggests that distortion reduction is a necessary but not a sufficient condition to completely stabilize the oscillation and ensure reproducibility. There are two other important instability mechanisms that we overlooked in the previous arguments.

First, perturbations arising from inherent noise and from reflections caused by imperfect terminations can excite various solitons in addition to the existing desired soliton pulse train. The perturbing solitons and the desired soliton train do not generally have the same amplitude (speed) and, therefore, collide with each other. These collisions cause significant amplitude and phase modulations, leading to unstable oscillations. Second, unless it is ensured that a single mode is generated every time (see Fig. 3 for possible mode examples), nonlinear intermode collisions on the NLTL, which occur due to the modes generally different amplitudes (speeds) could lead to instability. Summarizing, to attain a stable robust soliton oscillation with the circuit of Fig. 4, the amplifier should possess at least the following three capabilities:

1) distortion reduction;
2) perturbation rejection;
3) single mode selection.

Clearly, the voltage-limiting amplifier does not satisfy condition 1). Neither the voltage-limiting amplifier nor the linear amplifier satisfies 2) or 3), which will become evident in Section IV.

IV. NLTL Soliton Oscillator—Working Model

Our approach to attain a stable robust soliton oscillation with the circuit of Fig. 4 was the development of a unique amplifier. The amplifier incorporates an adaptive bias control that exploits the amplifier's nonlinear transfer function in order to allow the simultaneous satisfaction of the three stability requirements mentioned above. This section discusses the operating principle of our amplifier/oscillator.

A. Operating Principle

Our self-sustained soliton oscillator is schematically illustrated in Fig. 7. It is exactly the same topology as originally proposed in Fig. 4 and, interestingly, uses the voltage-limiting amplifier that was shown with Fig. 5 to cause apparently chaotic oscillations. The critical difference in our amplifier is that we operate it in a different region of its transfer curve to provide stability. This is done by using an adaptive bias control to move the amplifier bias point as the dc component of the amplifier output (V_Y in Fig. 7) changes. We will postpone the transistor-level description of the amplifier to Section IV-B. Here, we discuss how the transfer function of the amplifier together with the movable bias scheme allows us to simultaneously meet the three stability requirements.

Fig. 8(a) shows the transfer function of the amplifier. The transfer curve may be divided into the attenuation, gain, and voltage-limiting regions. In the attenuation region, the tangential

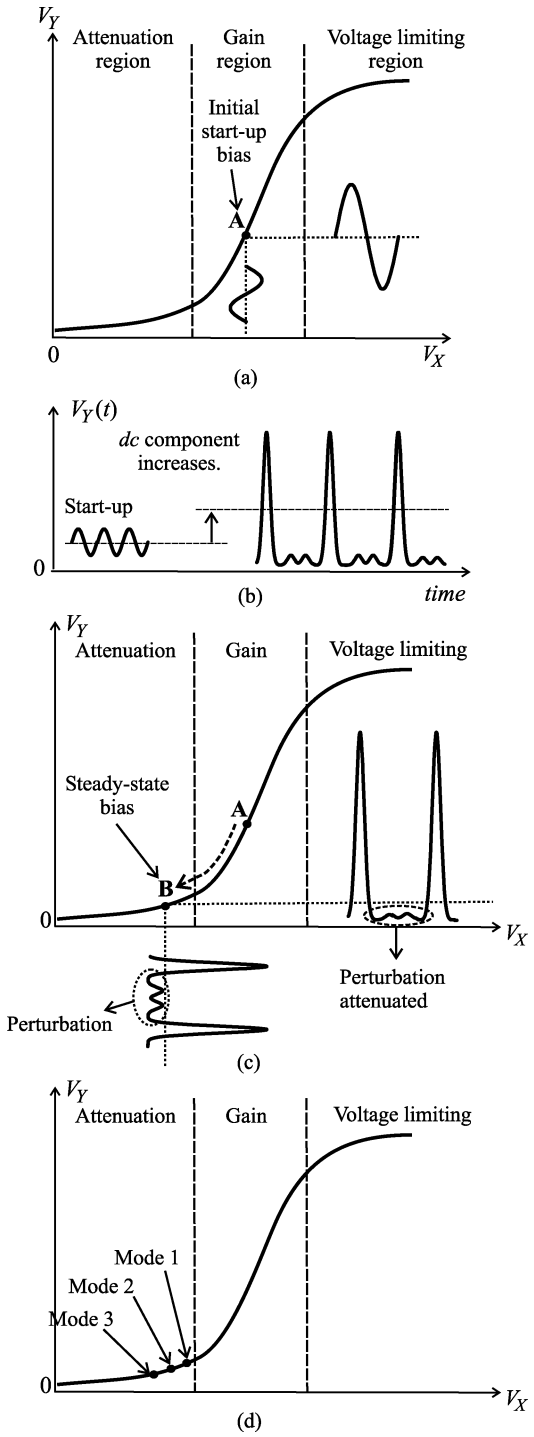

Fig. 8. (a) Nonlinear transfer curve of our amplifier. In the initial startup, bias point **A** lies in the gain region. (b) DC component of V_Y increases as the oscillation grows and forms into a soliton pulse train. (c) Increased dc component is used to lower the bias point of the amplifier, leading to a steady-state bias point **B**. (d) Mode-dependent steady-state bias.

slope at any point is less than 1 while in the gain region it is always greater than 1. In the voltage-limiting region, the tangential slope is also less than 1 but was termed the "voltage-limiting region" due to the clipping of large input voltages that fall in the region.

Initially, the amplifier is biased at **A** in the gain region, which allows startup from ambient noise. As the oscillation grows and forms into pulses, the dc component of $V_Y(t)$ steadily increases as illustrated in Fig. 8(b). The amplifier uses this increase in the dc component to lower its bias point, as is indicated with the broken arrow along the nonlinear transfer curve in Fig. 8(c). The reduced bias corresponds to a net *overall* gain reduction, since a portion of the pulse enters the attenuation region, thereby reducing the amount of the pulse that receives gain. The bias point keeps moving down on the transfer curve to the steady-state bias point **B** in the attenuation region, where the net overall gain of the amplifier becomes equal to the loss in the system. This adaptive bias control resolves all three issues mentioned in Section III-B.

Distortion Reduction: In the steady state shown in Fig. 8(c), the input bias has been sufficiently reduced so that the peak portions of the input and output pulses do not go into the voltage-limiting region of the amplifier transfer curve, thereby preventing significant signal distortion.

Perturbation Rejection: In the steady-state shown in Fig. 8(c), small perturbations at the input of the amplifier are attenuated at the output since they fall in the attenuation region of the transfer curve. This perturbation rejection is possible since the steady-state bias point **B** has been reduced into the attenuation region. However, the higher portions of the pulses lying in the gain region still receive enough gain to compensate loss.

This threshold-dependent gain-attenuation mechanism vital for stabilizing our soliton oscillator has been actually widely employed in optical mode-locked systems where it is known as *saturable absorption* [30], [31]. The saturable absorption technique has seen limited use in the electrical domain, and there only for linear-pulse oscillators [24], [32] (see Section VII).

It should be noted that we *avoid* the nonlinearity across the gain and voltage limiting regions in distortion reduction, but *exploit* the nonlinearity across the attenuation and gain regions for perturbation rejection.

Single Mode Selection: The single-mode selection is also made possible by the adaptive bias control. Since a higher mode has a higher dc component and correspondingly a lower steady-state bias due to the adaptive bias control [see Fig. 8(d)], the higher mode receives a lower gain. One can take advantage of this mode-dependent gain to select a particular mode. Only those modes with sufficient gain to overcome the loss of the system can be sustained in steady-state oscillations. When more than one mode has sufficient gain, only the highest mode is stable since any small perturbation to a lower mode will grow into a soliton, resulting in a higher mode oscillation. Consequently, the mode-dependent gain allows only one soliton propagation mode.

B. Example Amplifier Implementation

The amplifier concept described in the previous section is general and has a variety of different possible implementations. To provide an example of how to achieve the necessary amplifier functionality, we describe a specific amplifier implementation with MOS transistors (see Fig. 9) used in our low megahertz soliton oscillator prototype (see Section V). The amplifier consists of two inverting stages: one built around an nMOS transistor, M1, and the other built around a pMOS transistor M2. Together they form an overall noninverting active network. The

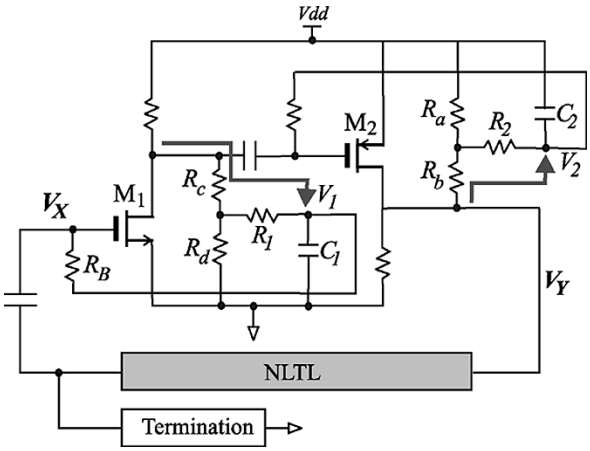

Fig. 9. Example amplifier implementation used.

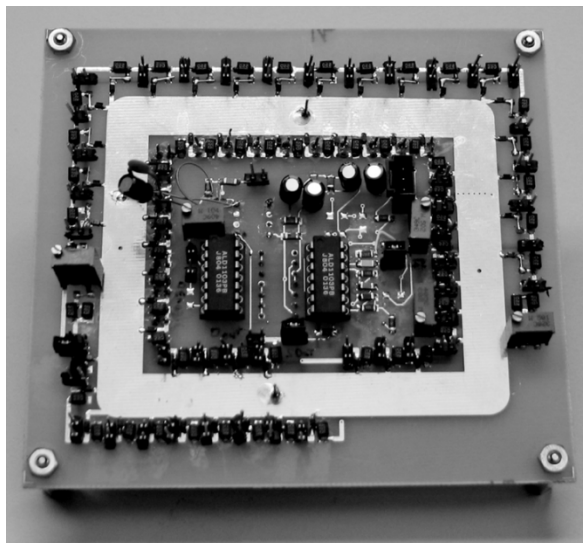

Fig. 10. Low megahertz soliton oscillator prototype.

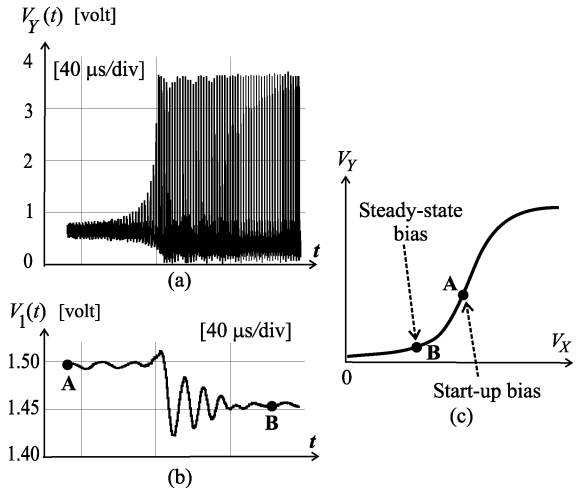

Fig. 11. (a) Measured voltage signal at the output of the amplifier during the oscillation startup transient. (b) Measured bias response $V_1(t)$ of the amplifier ($V_1(t)$ is with reference to Fig. 9) filtered by the oscilloscope with a 500-kHz bandwidth. $V_1(t)$ and $V_X(t)$ in the amplifier of Fig. 9 have the same dc component. (c) Redrawing of Fig. 8(c).

adaptive bias scheme is implemented for both inverting stages. It functions as follows for the pMOS stage. The output waveform V_Y is sensed by the voltage divider consisting of the two resistors R_a and R_b and then is integrated by the R_2-C_2 low-pass filter. The integrated voltage V_2 represents a scaled dc component of the waveform V_Y. This dc component is fed back to the gate of M2 to set its bias. As the dc level of V_Y increases, V_2 will rise with respect to ground. The increase in V_2 corresponds to a reduction in the gate–source voltage of M2, effectively lowering its bias. A similar argument applies to the nMOS stage. Combining the two stages, the bias of the amplifier at the input is reduced as the dc component of V_Y increases, performing the adaptive bias control described in the previous section.

V. Experimental Verification—Low Meghaertz Prototype

To demonstrate the concept of the electrical soliton oscillator, a low megahertz prototype shown in Fig. 10 was first constructed at the discrete board level (a microwave prototype will be presented in Section VI). In this prototype, lower frequency contents (the soliton pulse repetition rate of around 1 MHz and the soliton pulsewidth of about 100 ns) are chosen to facilitate the explicit oscilloscope measurement of various circuit nodes for rigorous proof of concept. An artificial NLTL consisting of discrete inductors and varactors (pn junction diodes) is used. The prototype produces a stable soliton pulse train after an initial pulse-forming transient process. In the following, we present a sequence of measurements that attest to the validity of the proposed circuit concept and design approach.

A. Adaptive Bias Control

Fig. 11(a) shows the voltage signal measured at the output of the amplifier during the oscillation startup transient, while Fig. 11(b) is the corresponding measured bias adjustment in the amplifier. As the oscillation grows and forms into soliton pulses, the amplifier self-adjusts to lower its bias according to the adaptive bias control scheme explained in Section IV-A. The bias point eventually settles to **B**, where the net overall gain of the amplifier becomes equal to the system loss. Fig. 8(c) is repeated in Fig. 11(c) for convenience and hypothetically illustrates the bias adjustment in the transient process. Note that the bias adjustment exhibits an under-damped response.

B. Startup Soliton Dynamics

Fig. 12 shows a detailed view of the oscillation startup measured at the eighth section on the NLTL (a total of 22 *LC* sections were used in this specific experiment to best illustrate the startup dynamics). The oscillator starts by amplifying ambient noise creating a small oscillation, eventually growing into a steady-state soliton pulse train. During this process, another competing mode is clearly seen: it first grows with time, but is eventually suppressed by the stabilizing mechanism of the amplifier. In the figure, one can also observe that the shorter pulse (competing mode) propagates at a different speed than the taller pulse (main mode that survives): in this time-domain measurement at the fixed point on the NLTL, the shorter pulse originally

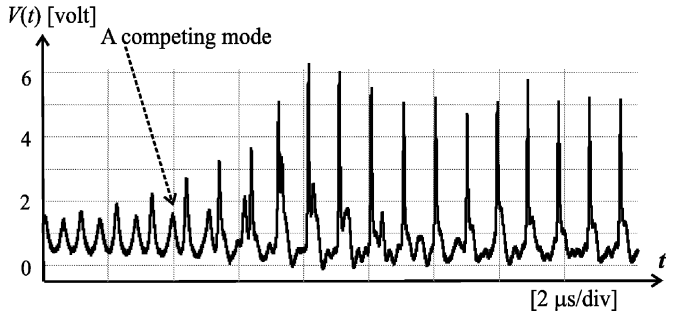

Fig. 12. Measured startup transient.

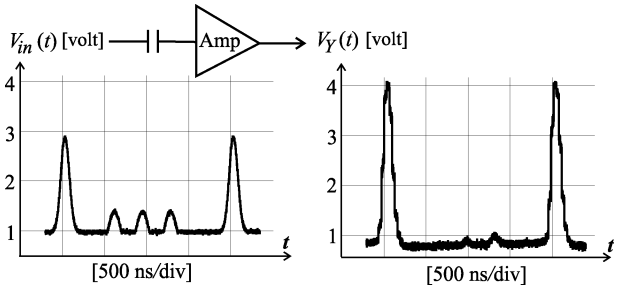

Fig. 13. Input–output measurements of the stand-alone amplifier biased at **B**.

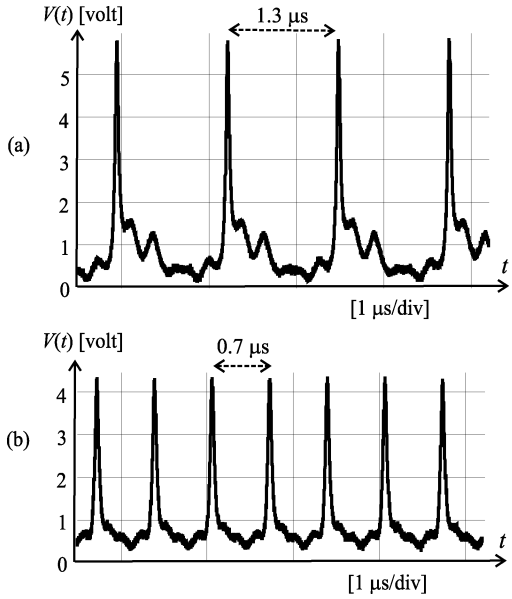

Fig. 14. Measured stable soliton oscillation in steady state. (a) $l = \Lambda$ oscillation. (b) $l = 2\Lambda$ oscillation.

behind the taller pulse catches up with the taller pulse and eventually moves ahead of it after collision. In the space domain, this corresponds to the taller pulse propagating faster than the shorter pulse, which is a key signature of solitons on the NLTL as explained in Section II.

C. Perturbation Rejection

Fig. 13 shows input–output measurements of the *stand-alone* amplifier when the amplifier is biased at its steady-state bias point **B**. The test input signal consists of two main pulses and perturbations between them. The perturbations are significantly attenuated at the output of the amplifier while the main pulses are amplified, due to the threshold-dependent gain-attenuation mechanism (e.g., saturable absorption, see Section IV-A). Note that, in addition to the perturbation attenuation, the amplifier has sharpened the main pulses. This is because the saturable absorption mechanism attenuates the lower portion of the input main pulses while amplifying their higher portion.

D. Steady-State Soliton Oscillation

Fig. 14(a) shows a steady-state soliton pulse train measured at the eighth section on the NLTL (30 *LC* sections in total). This waveform corresponds to the $l = \Lambda$ mode (Mode 1) shown in Fig. 3(b): at this mode, there exists only one pulse propagating around the NLTL. The measured period T_{mode1} for this particular mode was 1.3 μs.

By tuning the gain (bias), the $l = 2\Lambda$ mode (Mode 2) oscillation shown in Fig. 14(b) was controllably obtained. This mode corresponds to the $l = 2\Lambda$ mode (Mode 2) shown in Fig. 3(c), where two pulses copropagate in the NLTL. The measured period T_{mode2} for this mode was 0.7 μs. It is noteworthy that $2T_{\mathrm{mode2}} \neq T_{\mathrm{mode1}}$ while $2\Lambda_{\mathrm{mode2}} = \Lambda_{\mathrm{mode1}}$. This is because the two modes have different amplitudes and, hence, propagate at different speeds, which is another signature of the soliton propagation.

In both oscillation modes, the amplitude and pulse repetition rate remained stable and showed no discernable variation. Even when deliberately perturbed with large external signals, the oscillation always returned to the same steady-state soliton pulse train. Additionally, for a given set of circuit parameters, every start-up led to the same steady-state oscillation. These experiments demonstrate the level of robustness and controllability as found in traditional sinusoidal oscillators.

E. Spatial Dynamics in the Steady State

Fig. 15 shows the steady-state waveforms of the oscillator measured at three different *positions* on the NLTL. This experiment elucidates how the pulse shape changes as it circulates in the oscillator. The pulse at the output of the amplifier is not an exact soliton and, hence, sharpens into a soliton propagating down the NLTL. Once the soliton is formed at the eighth section, it exhibits damping soliton dynamics [26] as it further travels down the NLTL due to the loss, lowering in amplitude and velocity while increasing in width, as was explained in Section II. It is this clear existence of the transition point (eighth section) between the pulse sharpening and the stable damping that confirms the formation of the soliton at that transition point.

The measurement in Fig. 15 also shows that the amplifier sharpens the pulse from 110 ns FWHM to 100 ns FWHM. This narrowing by the amplifier is due to the saturable absorption, as mentioned earlier. However, it is important to note that, in our oscillator, the pulse sharpening by the NLTL (from 100 to 43 ns) is much more significant than the sharpening by the amplifier.

VI. Experimental Verification—Microwave Prototype

The soliton oscillator concept is general and the oscillator can be, in principle, scaled in frequency. To illustrate the frequency scalability of the circuit and demonstrate the design fea-

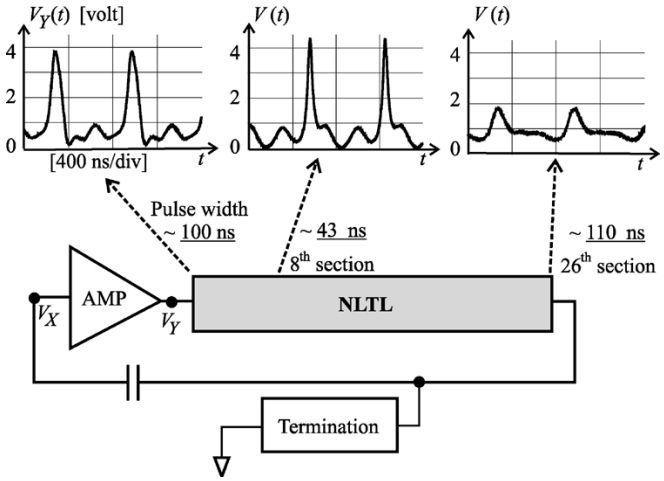

Fig. 15. Measured steady-state soliton oscillation at various points. Pulsewidth measured is the pulse full-width at half-maximum (FWHM) amplitude.

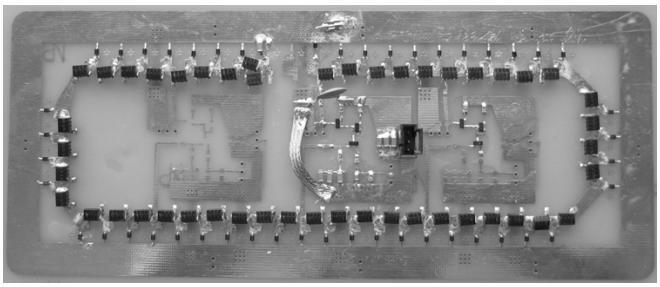

Fig. 16. Microwave soliton oscillator prototype.

sibility in the microwave region, the second prototype shown in Fig. 16 was constructed at the discrete board level. This prototype generates frequency content whose substantial portions lie in a lower microwave region. The amplifier in the microwave prototype is realized with RF bipolar transistors and performs the adaptive bias control on its nonlinear transfer curve, operating similarly to the MOS amplifier (see Section IV-B) used for the low megahertz prototype. An artificial NLTL is used where pn junction diodes are utilized as varactors.

The steady-state soliton oscillation from the second prototype is measured using an Agilent 54855A real-time oscilloscope and is shown in Fig. 17(a). A periodic soliton pulse train is clearly seen. The soliton pulse repetition rate is 130 MHz (which is inverse of the pulse repetition period 7.7 ns) while the soliton pulsewidth is 827 ps FWHM, which corresponds to a frequency well into the microwave region. The corresponding power spectral density (PSD) of the steady-state signal measured using the PSD measurement capability of the oscilloscope is shown in Fig. 17(b). The fundamental frequency of 130 MHz corresponds to the soliton repetition rate, as mentioned earlier. The significant harmonic content above 130 MHz is what determines the narrow soliton shape.

This prototype has demonstrated that the general soliton oscillator concept can be realized in a low microwave region. Implementations of the electrical soliton oscillator at even higher frequencies (possibly at a chip scale) would be a natural future extension of this study.

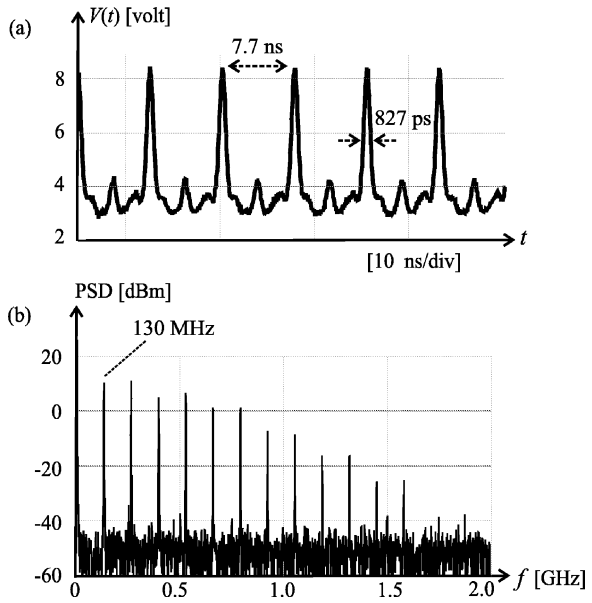

Fig. 17. Steady-state soliton oscillation from the microwave soliton oscillator prototype. (a) Time-domain (oscilloscope) measurement. (b) PSD obtained from the oscilloscope's PSD measurement capability.

VII. Comparison With Cutler's Work

In 1955, Cutler constructed a linear-pulse oscillator utilizing a circuit that has a similar topology as that in Fig. 4, but with a linear transmission line instead of the NLTL [24]. His amplifier, while based on vacuum tubes, incorporated the saturable absorption technique derived from a similar adaptive bias control. Cutler's work indeed marks the invention of the saturable absorption technique, while the name was coined later in optics [31]. Despite the fact that the basic operating principles of our amplifier and Cutler's amplifier are similar, Cutler's linear-pulse oscillator and our soliton oscillator have fundamentally different signal dynamics and design issues, as well as different physical implementations.

The most remarkable difference in design lies in the stability requirement. To stabilize oscillations, both oscillators rely on their amplifiers. However, our soliton oscillator has a much stronger tendency toward instability due to the nonlinear properties of the NLTL, as detailed in Section III-B. While noise and reflections are common sources of instability in both oscillators, nonlinear collisions and pulse breakup are unique features in the NLTL and are more difficult to stabilize. In addition, the reflections cannot be totally eliminated in the NLTL because of its voltage-dependent characteristic impedance. Therefore, the soliton oscillator demands significantly more from the amplifier's stabilizing function.

The signal dynamics of the two oscillators are significantly different as well. In Cutler's linear-pulse oscillator, the sharpening of the linear pulses is entirely executed by the amplifier through its saturable absorption function (as mentioned earlier, the saturable absorption performs not only perturbation rejection but also pulse sharpening). In our soliton oscillator, however, the NLTL is the dominant shaping and sharpening mechanism. Fig. 15 clearly shows that the sharpening by the NLTL is much more significant than that of the amplifier. Additionally, the sharpening-damping transition described in

Section V-E clearly demonstrates the unique properties of pulse propagation in the soliton oscillator, which cannot be seen in Cutler's linear oscillator.

A historical reflection of the development of the saturable absorption technique may provide another perspective into the relation between our and Cutler's work. While born in electronics by Cutler in 1955, the saturable absorption technique was soon adopted into optics in 1966 [31] for optical linear-pulse oscillators, receiving its popular name, saturable absorption. After the discovery of the optical soliton [9], the technique was further developed in 1992 to enable optical *soliton* oscillators, e.g., fiber ring laser [33], [34]. The development of the saturable absorption technique in optics has paved the way for the expansive field of optical mode-locking [30]. In contrast, the saturable absorption technique has been rarely applied in its native electronics domain to the best of the authors' knowledge, with its application limited to a few electrical linear-pulse oscillators [24], [32]. The work presented in this paper makes the transition from the electrical linear-pulse oscillator to the electrical soliton oscillator, mirroring the transition already made in optical mode locking.

VIII. Conclusion

In this paper, we presented the first robust electrical soliton oscillator with full experimental demonstration. The oscillator is a one-port system that self-generates a periodic soliton pulse train from ambient noise. The soliton oscillator consists of an NLTL and a nonlinear amplifier utilizing an adaptive bias control. The NLTL is responsible for soliton formation. The amplifier is responsible for the initiation of startup, compensation of loss, and stabilization of oscillation in the steady state. The soliton oscillator is a direct analog of the optical soliton mode-locked system such as a fiber ring laser.

The focus of this paper was on the introduction of the new soliton oscillator concept and not a specific design at a certain frequency. The two prototypes presented in this paper demonstrated that the concept is general and scalable in frequency. This work henceforth lays the foundation for further study of electrical soliton oscillators (electrical soliton mode locking). Implementations of the soliton oscillator at a chip scale to achieve a higher speed performance (narrower pulsewidth) will be the most significant engineering direction. The electrical soliton oscillators may add a valuable direction in the field of high-speed metrology and microwave sampling [18]–[20].

Acknowledgment

The authors would like to thank M. DePetro, Harvard University, Cambridge MA, for his significant efforts in fabricating the low megahertz prototype. The authors would also like to thank Dr. G. Ballantyne, Qualcomm, Christchurch, New Zealand, and Prof. D. Taylor, University of Canterbury, Canterbury, New Zealand, for their discussions and encouragement and L. DeVito, R. Sullivan, and S. Feindt, all of Analog Devices Inc., Wilmington, MA, for their continued support and help with experiments. The authors would also like to thank W. Andress, K. Woo, M. Taghivand, M. A. Belabbas, and Prof. R. Brockett, all of Harvard University, Cambridge, MA, for their valuable suggestions. The authors further acknowledge Sonnet Software, North Syracuse, NY, the Ansoft Corporation, Pittsburgh, PA, for their donated EM field solvers, and Agilent EEsof EDA, Palo Alto, CA, for their donated ADS software.

References

[1] A. C. Scott, F. Y. F. Chu, and D. W. McLaughlin, "The soliton: A new concept in applied science," *Proc. IEEE*, vol. 61, no. 10, pp. 1443–1483, Oct. 1973.

[2] N. J. Zabusky and M. D. Kruskal, "Interactions of solitons in a collisionless plasma and the recurrence of initial states," *Phys. Rev. Lett.*, vol. 15, no. 6, pp. 240–243, 1965.

[3] P. G. Drazin and R. S. Johnson, *Solitons: An Introduction*. Cambridge, U.K.: Cambridge Univ. Press, 1989.

[4] A. T. Filippov, *The Versatile Soliton*. Boston, MA: Birkhauser, 2000.

[5] M. Remoissenet, *Waves Called Solitons: Concepts and Experiments*. New York: Springer-Verlag, 1999.

[6] J. S. Russel, "Report on waves," in *Report 14th British Assoc. Advancement of Science Meeting*, York, U.K., Sep. 1844, pp. 311–390.

[7] E. Fermi, J. Pasta, and S. Ulam, "Studies of nonlinear problems. I," Los Alamos Sci. Lab., Los Alamos, NM, Tech. Rep. LA-1940, 1955.

[8] A. C. Newell, *Nonlinear Wave Motion*. Providence, RI: Amer. Math. Soc., 1974.

[9] A. Hasegawa and F. Tappert, "Transmission of stationary nonlinear optical pulses in dispersive dielectric fibers. I. Anomalous dispersion," *Appl. Phys. Lett.*, vol. 23, no. 3, pp. 142–144, Aug. 1973.

[10] R. Hirota and K. Suzuki, "Theoretical and experimental studies of lattice solitons in nonlinear lumped networks," *Proc. IEEE*, vol. 61, no. 10, pp. 1483–1491, Oct. 1973.

[11] M. J. Rodwell, S. T. Allen, R. Y. Yu, M. G. Case, U. Bhattacharya, M. Reddy, E. Carman, M. Kamegawa, Y. Konishi, J. Pusl, and R. Pullela, "Active and nonlinear wave propagation devices in ultrafast electronics and optoelectronics," *Proc. IEEE*, vol. 82, no. 7, pp. 1037–1059, Jul. 1994.

[12] J. R. Alday, "Narrow pulse generation by nonlinear transmission lines," *Proc. IEEE*, vol. 22, no. 6, p. 739, Jun. 1964.

[13] D. W. van der Weide, "Delta-doped schottky diode nonlinear transmission lines for 480-fs, 3.5-V transients," *Appl. Phys. Lett.*, vol. 65, no. 7, pp. 881–883, Aug. 1994.

[14] M. J. W. Rodwell, M. Karnegawa, R. Yu, M. Case, E. Carman, and K. S. Giboney, "GaAs nonlinear transmission lines for picosecond pulse generation and millimeterwave sampling," *IEEE Trans. Microw. Theory Tech.*, vol. 39, no. 7, pp. 1194–1204, Jul. 1991.

[15] M. G. Case, "Nonlinear transmission lines for picosecond pulse, impulse and millimeter-wave harmonic generation," Ph.D. dissertation, Dept. Elect. Comput. Eng., Univ. California at Santa Barbara, Santa Barbara, CA, 1993.

[16] H. Shi, W.-M. Zhang, C. W. Dornier, N. C. Luhmann Jr., L. B. Sjogren, and H.-X. L. Liu, "Novel concepts for improved nonlinear transmission line performance," *IEEE Trans. Microw. Theory Tech.*, vol. 43, no. 4, pp. 780–789, Apr. 1995.

[17] D. Salameh and D. Linton, "Microstrip GaAs nonlinear transmission-line (NLTL) harmonic and pulse generators," *IEEE Trans. Microw. Theory Tech.*, vol. 47, no. 7, pp. 1118–1122, Jul. 1999.

[18] M. Kahrs, "50 years of RF and microwave sampling," *IEEE Trans. Microw. Theory Tech.*, vol. 51, no. 6, pp. 1787–1805, Jun. 2003.

[19] R. Y. Yu, M. Reddy, J. Pusl, S. T. Allen, M. Case, and M. J. W. Rodwell, "Millimeter-wave on-wafer waveform and network measurements using active probes," *IEEE Trans. Microw. Theory Tech.*, vol. 43, no. 4, pp. 721–729, Apr. 1995.

[20] R. Y. Yu, J. Puls, K. Yoshiyuki, M. Case, K. Masayuki, and M. Rodwell, "A time-domain millimeter-wave vector network analyzer," *IEEE Microw. Guided Wave Lett.*, vol. 2, no. 8, pp. 319–321, Aug. 1992.

[21] G. J. Ballantyne, P. T. Gough, and D. P. Taylor, "Periodic solutions of Toda lattice in loop nonlinear transmission line," *Electron. Lett.*, vol. 29, no. 7, pp. 607–609, Apr. 1993.

[22] ——, "A baseband soliton oscillator," *Chaos, Solitons Fractals*, vol. 5, no. 6, pp. 1013–1029, Jun. 1995.

[23] G. J. Ballantyne, "Periodically amplified soliton systems," Ph.D. dissertation, Dept. Elect. Electron. Eng., Univ. Canterbury, Christchurch, New Zealand, 1994.

[24] C. C. Cutler, "The regenerative pulse generator," *Proc. IRE*, vol. 43, pp. 140–148, Feb. 1955.

[25] D. S. Ricketts, X. Li, M. DePetro, and D. Ham, "A self-sustained electrical soliton oscillator," in *IEEE MTT-S Int. Microwave Symp. Dig.*, Jun. 2005, pp. 1365–1368.
[26] E. Ott and R. N. Sudan, "Damping of solitary waves," *Phys. Fluids*, vol. 13, no. 6, pp. 1432–1434, Jun. 1970.
[27] M. Toda, *Theory of Nonlinear Lattices*. New York: Springer-Verlag, 1981.
[28] D. Ham and A. Hajimiri, "Concepts and methods in optimization of integrated *LC* VCOs," *IEEE J. Solid-State Circuits*, vol. 36, no. 6, pp. 896–909, Jun. 2001.
[29] W. Andress and D. Ham, "Standing wave oscillators utilizing wave-adaptive tapered transmission lines," *IEEE J. Solid-State Circuits*, vol. 40, no. 3, Mar. 2005.
[30] H. A. Haus, "Mode-locking of lasers," *IEEE J. Sel. Topics Quantum Electron.*, vol. 6, no. 6, pp. 1173–1185, Nov./Dec. 2000.
[31] A. J. DeMaria, D. A. Stetser, and H. Heynau, "Self mode-locking of lasers with saturable absorbers," *Appl. Phys. Lett.*, vol. 8, no. 7, pp. 174–176, Apr. 1966.
[32] L. A. Glasser and H. A. Haus, "Microwave mode locking at X-band using solid-state devices," *IEEE Trans. Microw. Theory Tech.*, vol. MTT-26, no. 2, pp. 62–69, Feb. 1978.
[33] K. Tamura, H. A. Haus, and E. P. Ippen, "Self-starting additive pulse mode-locked erbium fiber ring laser," *Electron. Lett.*, vol. 28, no. 24, pp. 2226–2228, Nov. 1992.
[34] C. J. Chen, P. K. A. Wai, and C. R. Menyuk, "Soliton fiber ring laser," *Opt. Lett.*, vol. 17, no. 6, pp. 417–419, Mar. 1992.

David S. Ricketts (S'98) received the B.S. and M.S. degrees in electrical engineering from Worcester Polytechnic Institute, Worcester, MA, and is currently working toward the Ph.D. degree at Harvard University, Cambridge, MA.

From 1995 to 1999, he was involved with the power electronics industry, developing high-efficiency dc–ac converters, and power-management integrated circuits. From 1999 to 2003, he worked for a variety of semiconductor companies as a Principle Design Engineer, Product Development Manager, and Strategic Marketing Manager. In 2003, he joined the Division of Engineering and Applied Sciences, Harvard University. His research interests include RF integrated-circuit design, silicon nanowire circuits, and nonlinear wave-based circuits and systems.

Mr. Ricketts was a 2004 Innovation Fellow at Harvard University. He was the recipient of the 2006 Analog Devices Outstanding Student Designer Award. He was also the recipient of the Analog Devices Fellowship presented by the Worcester Polytechnic Institute.

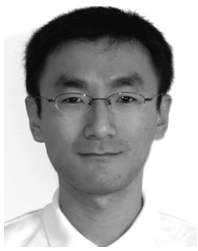

Xiofeng Li (S'05) was born in Luoyang, China. He received the B.S. degree from the California Institute of Technology, Pasadena, in 2004, and is currently working toward the Ph.D. degree at Harvard University, Cambridge, MA.

His main research interest lies in the design and experimentation of gigahertz-to-terahertz ultrafast quantum circuits using nanoscale devices such as quantum dots, nanowires, and carbon nanotubes.

Mr. Li was recipient of a Gold Medal at the 29th International Physics Olympiad, Reykjavik, Iceland, 1998. He ranked first (absolute winner) in the Boston Area Undergraduate Physics Competition in both 2001 and 2002. He was also the recipient of the 2004 Harvard University Pierce Fellowship and the 2005 Analog Devices Outstanding Student Designer Award.

Donhee Ham (M'02) received the B.S. degree in physics from Seoul National University, Seoul, Korea, in 1996, and the Ph.D. degree in electrical engineering from the California Institute of Technology, Pasadena, in 2002.

From 1997 to 1998, he was with the Laser Interferometer Gravitational Wave Observatory (LIGO), Pasadena, CA. In 2000, he was with the IBM T. J. Watson Research Center, Yorktown Heights, NY. In 2002, he joined the Faculty of the Division of Engineering and Applied Sciences, Harvard University, Cambridge, MA, as an Assistant Professor of electrical engineering. His research focus is on ultrafast electronics, specifically RF and microwave integrated circuits, soliton and nonlinear wave electronics, and nanoscale quantum-effect devices for gigahertz and terahertz circuits. His research also examines biological laboratories on an integrated circuit.

Mr. Ham ranked first in the School of Natural Science, Seoul National University upon his graduation. He was the recipient of the Presidential Top Honor Prize. He was a recipient of the Li Ming Scholarship and IBM Research Fellowship presented by the California Institute of Technology. He was the recipient of the 2002 California Institute of Technology Charles Wilts Doctoral Thesis Prize for outstanding Ph.D. research in electrical engineering. He was also the recipient of the 2003 IBM Faculty Partnership Award.